JOURNAL OF MECHANICAL ENGINEERING AND SCIENCES (JMES)
ISSN: 2289-4659 e-ISSN: 2231-8380
VOL. 14, ISSUE 3, 7181 – 7190
DOI: https://doi.org/10.15282/jmes.14.3.2020.19.0564

ORIGINAL ARTICLE

Effect of dome size on flow dynamics in saccular aneurysms – A numerical study

S. Nayak[1], N. Kumar[1*], S. M. A. Khader[1] and R. Pai[1]

[1] Department of Mechanical and Manufacturing Engineering, Manipal Institute of Technology, Manipal Academy of Higher Education, Manipal-576104, India
Phone: +91 74111 49954

ABSTRACT – Image-based Computational Fluid Dynamic (CFD) simulations of anatomical models of human arteries are gaining clinical relevance in present days. In this study, CFD is used to study flow behaviour and hemodynamic parameters in aneurysms, with a focus on the effect of geometric variations in the aneurysm models on the flow dynamics. A computational phantom was created using a 3D modelling software to mimic a spherical aneurysm. Hemodynamic parameters were obtained and compared with the available literature to validate. Further, flow dynamics is studied by varying the dome size of the aneurysm from 3.75 mm to 6.25 mm with an increment of 0.625 mm keeping the neck size constant. The aneurysm is assumed to be located at a bend in the arterial system. Computational analysis of the flow field is performed by using Navier – Stokes equation for laminar flow of incompressible, Newtonian fluid. Parameters such as velocity, pressure, wall shear stress (WSS), vortex structure are studied. It was observed that the location of the flow separation and WSS vary significantly with the geometry of the aneurysm. The reduction of WSS inside the aneurysm is higher at the larger dome sizes for constant neck size.

ARTICLE HISTORY
Revised: 18th Mar 2020
Accepted: 21st Mar 2020

KEYWORDS
Computational fluid dynamics;
aneurysm;
wall shear stress;
velocity vectors;
dome size

INTRODUCTION

Aneurysms are vascular tissue where there is a weakness in the arterial wall leading to localized dilation or ballooning in the artery. The blood flow within the artery impinges against the thinned region of the wall, leading to the formation of an aneurysm. As the arterial wall becomes thinner due to dilation, the flow causes the weakened wall to swell. This may lead to rupture of the aneurysm leading to haemorrhage. Saccular aneurysm is one of the most common types accounting for more than 70% of all intracranial aneurysm and one of the most common non-traumatic subarachnoid haemorrhage. This kind of aneurysm looks like a sac at the bifurcations of arteries, usually at the circle of willis [1]. Wall shear stress and structural property of the artery are predominant factors for the rupture to occur. Wall shear stress is mainly dependent upon wall property, aneurysm geometry and internal pressure in the aneurysm [2]. Stress inside the aneurysm will affect the arterial wall permeability and transport between lumen and wall. Biomechanical factors are activated by the endothelial cells because of hemodynamic changes. This adaptation will degrade the arterial wall resulting in the growth of the aneurysm.

Hoi et al. [3] observed that the growth of the aneurysm is dependent on the arterial curvature and the neck size. This was proved by Sato et al. [4] who studied the importance of arterial geometry and intra-aneurysmal hemodynamics by using the parametric model of the aneurysm with different aneurysm shapes. Imai et al. [5] suggested that it is important to consider arterial geometry and secondary flow in the design of endovascular devices by analysing the steady-state inflow for aneurysms. Thenier et al. [6] carried out the research work considering the patient-specific cases and observed the presence of lower wall shear stress in the ruptured aneurysms. The study conducted by Sano et al. [7] highlights the relevance of the idealised model to reveal the hemodynamic characteristics to understand the rupture status. Method of clustering the time-dependent blood flow data in cerebral aneurysm was presented by Meuschke et al. [8] which help in classification of aneurysms based on flow patterns. Lijian Xu et al [9] discussed the relevance of CFD based analysis in the selection and optimization of flow diverter devices. Flow diverter devices are widely used in the treatment of cerebral aneurysms. Janiga et al. [10] carried out the three-dimensional CFD based simulation of virtual deployment of an uncompressed flow diverter in patient-specific aneurysm models and observed a significant reduction in blood flow into the aneurysm. A large number of numerical simulation study of bell-shaped stenosed artery have been carried out by Goswami et al. [11] for the investigation of fluid mechanical factors. It was found that the possibility of increase of plaque deposition at the downstream of the stenosis increase with the increase in Reynolds number and Womersley number of the flow.

Many researchers have studied the flow dynamics in aneurysms after stenting. Hassan et al. [12] discussed the effect of a single and double stent on the circumferential pressure distribution and observed that the deployment of the stent affected the aneurysm and suggested to choose the stent depending on the type of aneurysm. Kim et al. [13] numerically studied the effect of strut shape and porosity on the hemodynamic parameters inside the aneurysms. Babiker et al. [14] analysed the quantitative effects of the density of the coil packing inside the aneurysm by in-vitro flow study.

*CORRESPONDING AUTHOR | N. Kumar | ✉ nitesh.naik@manipal.edu

Several attempts have been made to find the relation between arterial geometry and rupture risk by analysing parameters such as size, shape, etc.[15]–[18]. In this study, computational parametric investigation of blood flow in the idealised saccular aneurysm is presented. The variation of the flow pattern and the hemodynamic parameters with the variation in dome size on the intra-aneurysmal flow is enumerated. The aneurysm is assumed located at the bend of the artery. The flow parameters are analysed computationally. Circular neck and dome sizes are considered, and dome size is varied in different models keeping neck size as constant. Hemodynamic parameters such as velocity and wall shear stress are considered for characterization of the flow field.

COMPUTATIONAL DOMAIN

The saccular aneurysm consists of a balloon-like sac, with a constricted neck. The geometric parameters governing the size of the aneurysm are sac diameter D and neck diameter N. The flow inside the aneurysm is dependent upon the shape and size of the aneurysm and also the artery. The flow varies due to change in the shape of the aneurysm dome and neck and also the diameter of the parent artery [19].

The flow characteristics vary significantly inside the aneurysm as the flow pattern depends on the shape and size of the aneurysm. Flow varies greatly due to variation in neck size, dome diameter, angle at which blood enters the aneurysm, aneurysm shape and size. Study on patient-specific aneurysm models in the analysis of hemodynamic parameter variation was carried out by many researchers. However, idealised geometrical models were considered, because a parametric study using idealised models can clearly reveal the effect of geometric characteristics on the flow pattern. The model of the aneurysm was according to the theory described by Parlea et al. [17].

Five aneurysm model geometries with the constant neck size and varying dome diameter are considered in this study. The geometry of these models is similar to the geometry described by G. Mulder et al. [2]. The neck diameter was kept constant by varying the dome diameters. The neck diameter was 2.5mm, constant for all models and Diameter to neck ratio ranging from 1.5 to 2.5 with an increment of 0.25 mm. Figure 1 and Table 1 highlight the dimensions used in the present study.

Table 1. Dome and Neck diameters of different models having different D/N ratio

D/N Ratio	Neck diameter, ΦN (mm)	Dome diameter, ΦD (mm)
1.5	2.5	3.75
1.75	2.5	4.375
2	2.5	5
2.25	2.5	5.625
2.5	2.5	6.25

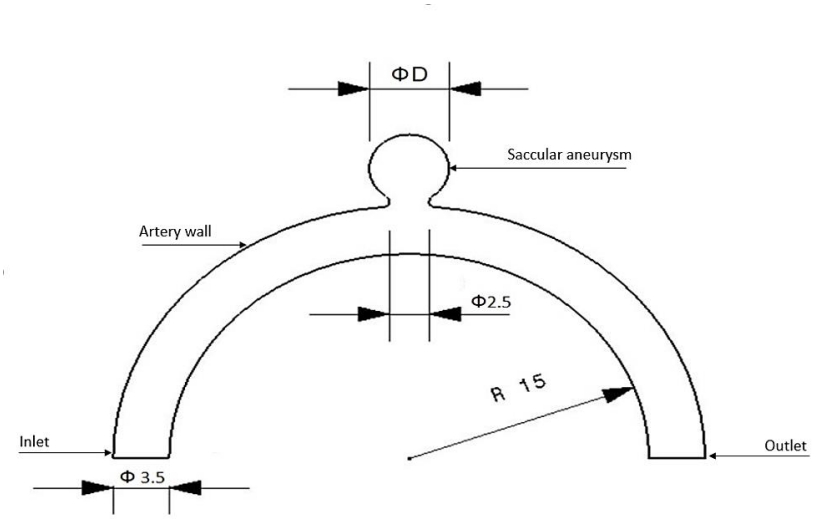

Figure 1. Dimensions of the idealised aneurysm model used in the present study

MATERIALS AND METHODS

Sudo et al. [20] discussed fully developed flow in a circular pipe. It was observed that if Dean Number is less than 100 the curvature effects can be neglected. The secondary flow was classified into five groups and one of them is Dean circulation having Dean number less than 100 and Womersley number less than 5.5. The Dean number and Womersley

number calculated for the models are found to be 96 and 1.81. It was shown that the vortex of secondary flow does not shift during a pulsatile cycle because of the viscous effect which moves to the center of the vessel due to low Dean number and Womersley number is less than 5, the pulsatile flow can be considered as laminar and steady. However, the pulsatile flow condition is more appropriate to describe the flow of blood but computationally expensive. As per the study conducted by Geers et al. [21], steady flow simulations can accurately approximate the WSS field of the aneurysm. So, in this study, the steady laminar flow was considered with an average Reynolds number of 285.

The flow of blood is governed by the Navier Stokes equation. The conservation of mass and momentum for an incompressible fluid in three dimensions is given as:

$$\nabla . v = 0 \tag{1}$$

$$\rho((\partial v/\partial t) + v\,\nabla v) = \nabla p + \nabla \tau \tag{2}$$

where ρ is the constant density, v is the velocity vector, p is the pressure and τ is the shear stress tensor.

Ku et al. [22] suggest that for the large arteries, the Reynolds number ranges from 110 to 850 so that the non-Newtonian effect is not appreciable for blood [23]. Blood was assumed as Newtonian, incompressible fluid where the density is taken as 1080 kg/m^3. The flow rate in 3.5mm parent artery is 2.88ml/s with the constant inlet velocity of 0.3 m/s and the viscosity of the blood is taken as 0.004 Pa-s [24]. Wall is assumed to be rigid [25] and the no-slip condition is applied at the wall. Poiseuille velocity profile was applied at the inlet and zero pressure at the outlet. The 3D unsteady Navier Stokes equations were solved by implementing a finite volume scheme using ANSYS Fluent (ANSYS Inc., Canonsburg, PA).

Accuracy of any numerically simulated studies mainly depends upon the quality of the mesh [26]. An appropriate number of control volumes can resolve the numerical equations and effectively capture the hemodynamics at various locations in the computational model used in this study. The grid independence test is performed to check the quality of the mesh for solution convergence by varying the number of control volumes in the computational domain. Grid independence test carried out for all aneurysm models adopted in the CFD study to optimise the element size for every aneurysm model and it is shown in Figure 3. A laminar flow model was used to simulate the steady flow in the carotid arteries with an RMS value of 10^{-4} [27]. A maximum of 600 iterations was taken for convergence in the study. In this study, the tetrahedral mesh was used with the number of elements ranging from 6,00,000 to 8,00,000. A close view of the tetrahedron mesh is shown in Figure 4.

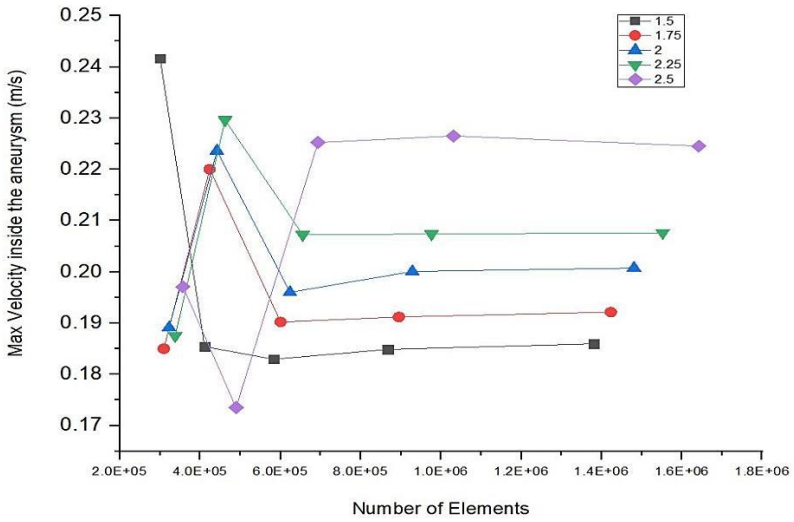

Figure 2. Grid independence study result for different models

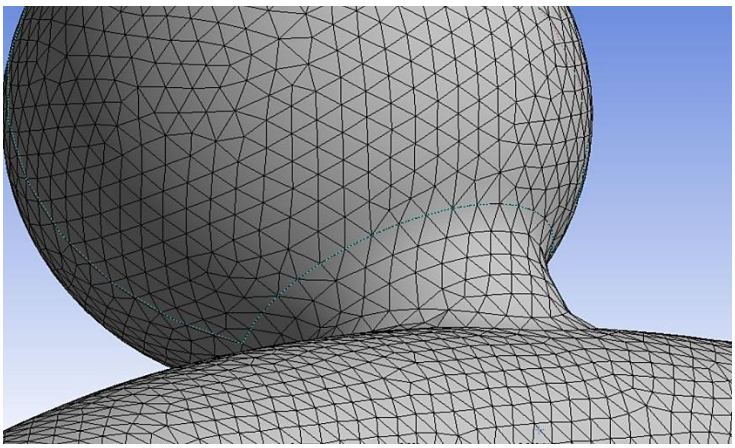

Figure 3. Tetrahedron meshing

VALIDATION

In the present study, since the focus is on the idealised aneurysm in arterial bend, initially a steady-state validation was performed and the results are compared with experimental studies performed by Zhang et al. [28]. Figure 4 represents the grid independence test results carried out for the Yi-Sen model. Tetrahedron mesh with 7,50,000 number of elements was used. A laminar flow model was used to simulate the steady flow. Maximum velocity, wall shear stress and average velocity at the midplane of the aneurysm are considered in the study. Table 2 shows the comparison of results between the present study and the literature which is agreeing well.

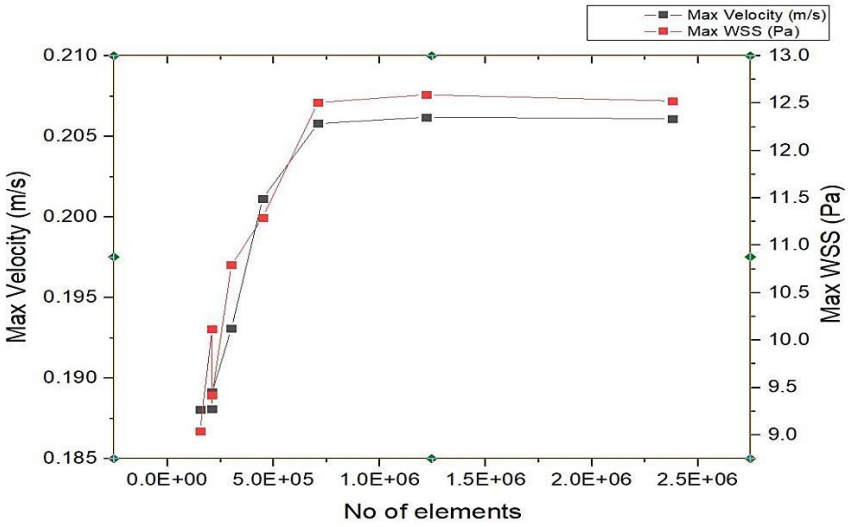

Figure 4. Grid independence study for Yi-sen model

Table 2. Comparison of results between Yi-Sen model and the present study

Hemodynamic Parameters	Yi-sen model	Present Study
Maximum Velocity (V_{max}), in m/s	0.2089	0.2058
Wall Shear Stress (WSS), in Pa-s	1.2351	1.2701
Average Velocity (V_{avg}), in m/s	0.0550	0.054

RESULTS AND DISCUSSION

To acquire the results from the CFD simulation, a plane was considered at the midplane of the artery bisecting the aneurysm laterally as shown in Figure 4. Hemodynamic parameters such as velocity, WSS were calculated for the models with different dome sizes. The flow from the main artery meets the neck at the downstream side. The flow then divides and enters the aneurysm with significantly low velocity and produces vortex inside the aneurysm. A portion of the flow

proceeds along the main artery. Figure 5 shows the plane sections of the models considered in the study. Two plane sections, one at the mid-plane and another at the neck of the aneurysm are considered.

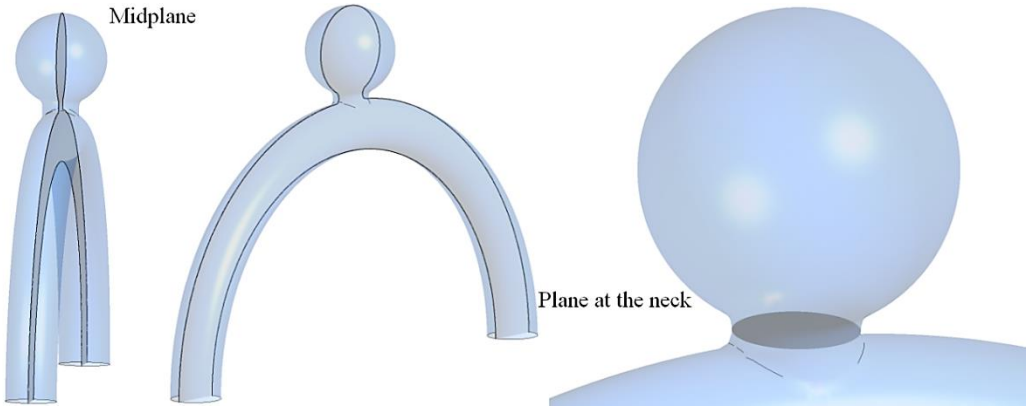

Figure 5. Section planes along the midplane and across the neck

The fluid enters the aneurysm and circulates inside the sac of the aneurysm. Double vortices were not observed in the aneurysm. According to Ujiie et al. [29], a double vortex was observed in the aneurysm at bifurcations. Figure 6 shows the velocity contours for different aneurysm models. It can be observed that as the dome size increases the velocity magnitude decreases in the region above the neck. The velocity magnitude inside the dome is smaller than the parent artery. It can also be observed that the velocity pattern is varying with the variation in dome size. The area-averaged velocity considered over the mid-sectional area of the aneurysm dome is also observed in Figure 6. The area-averaged velocity is higher in the case of the aneurysm with lesser dome diameter. The calculated reduction of area-averaged velocity is 94% in the case of D/N=1.5. This reduction is higher in the models having higher dome diameter and up to 97% reduction in area-averaged velocity is found in the case of D/N = 2.5. There is 94.5% reduction in maximum velocity observed inside the aneurysm. The blood entering the dome has a lesser velocity at the top of the dome and a portion of blood remain stagnant at the apex of the dome. This stagnation is higher in the case of higher dome sizes. The area-averaged velocity is taken over the aneurysm dome midplane area, the blood stagnation area is higher for larger domes. The velocity magnitude is smaller than the parent artery and the low-velocity magnitude leads to low WSS inside the dome of the aneurysm as observed in Figure 6.

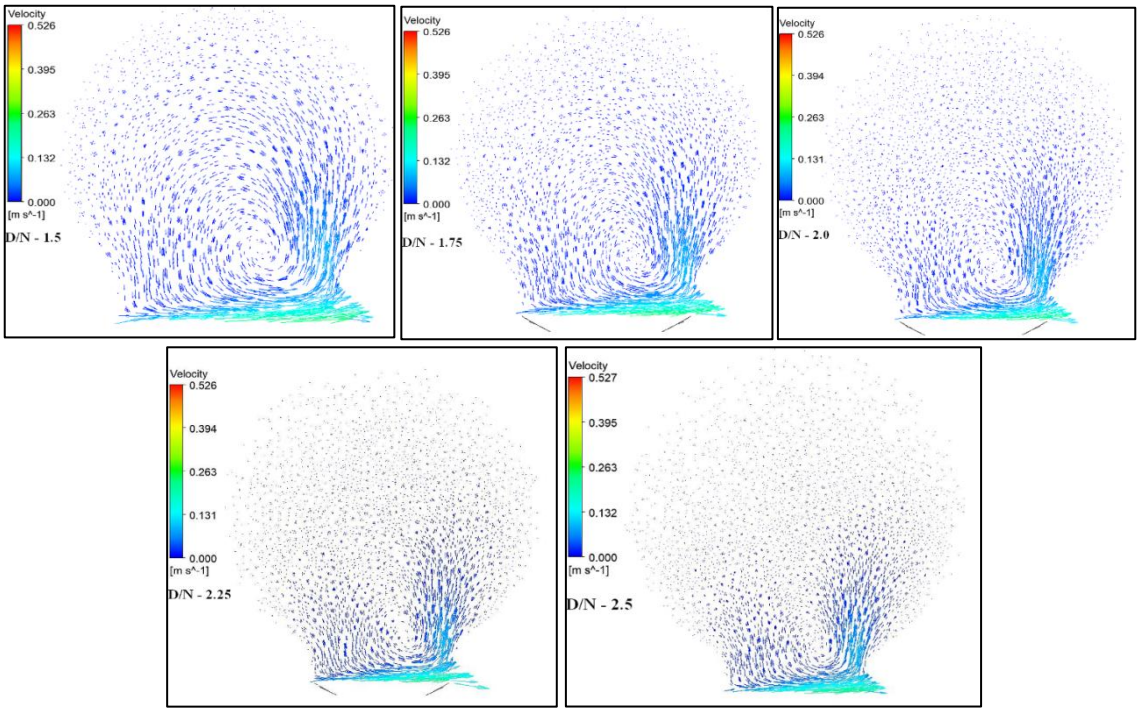

Figure 6. Velocity vectors for different aneurysm models

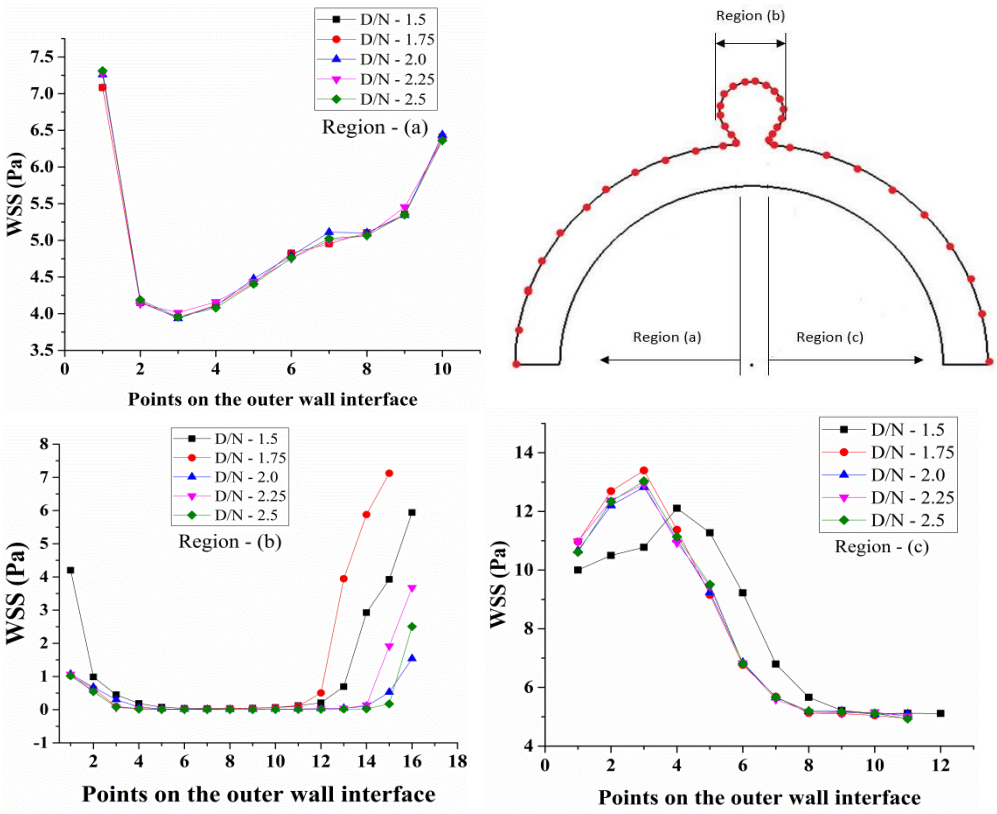

Figure 7. WSS at different regions of the model: (a) WSS at region a, (b) WSS at region b and (c) WSS at region c

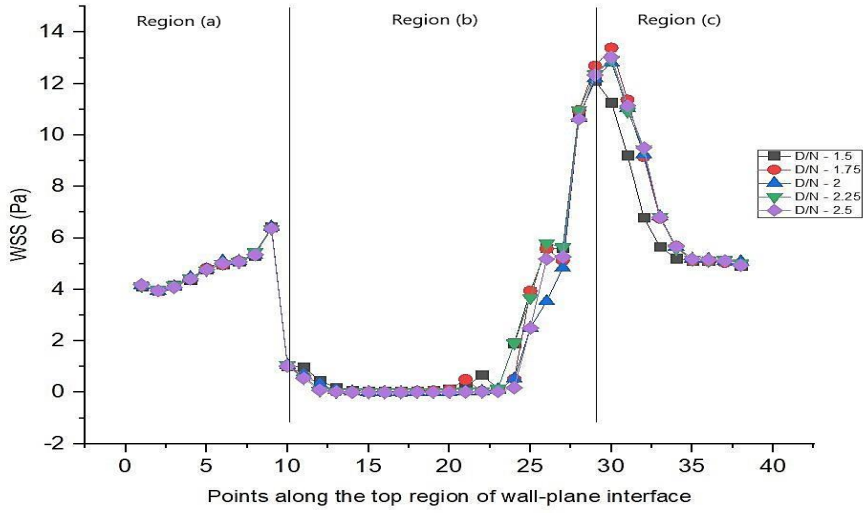

Figure 8. Wall Shear Stress (WSS) at the top region of wall and mid-plane interface

Figure 7(a), (b) and (c) represent the wall shear stress at different regions of the model. The different regions of the model considered is shown in Figure 7. It was observed by Malek et al. [30] that the low WSS at the walls of the aneurysm leads to the development of atherosclerosis. The variation pattern is observed to be similar in case of all the models. Figure 7(a) represents the wall shear stress at the region (a) shown in Figure 7. Region (a) is the section from inlet to the proximal side of the aneurysm neck. There is a gradual increase of WSS from the inlet up to the last probe point of region (a). There is a flow impingement at the distal side of the aneurysm neck and a small portion of the blood enters the aneurysm dome and the rest flow through the main artery. The variation of WSS inside the dome is represented in Figure 7(b), considering the probe points on the aneurysm wall in the clockwise direction. Among the 15 probe points considered on the wall of the aneurysm dome, the points near the distal side of the dome showed increasing WSS. A local maximum WSS was shown at the distal side of the aneurysm dome but the points on the top and proximal sections of the aneurysm dome showed decreasing WSS. The differences in the WSS arise due to the differences in the velocity patterns. The

increase in WSS is due to the higher velocity of the flow. The lowest WSS is observed at the top of the dome. WSS reaches a maximum value at the region (c) as shown in Figure 7(c). Then the WSS gradually decreases along with the points on the wall up to the outlet.

Figure 8 shows the variation of WSS along the wall of the artery and aneurysm at the wall and mid-plane interface. The wall shear stress inside the aneurysm reduces to 0.004Pa at the top region of the dome which is around 94% lesser than the WSS at the arterial wall. The velocity magnitude attenuates as the flow reaches the apex of the dome. The variation in the WSS is due to the differences in velocity magnitude. The blood flow entering the aneurysm forms vortex over the luminal surface. The luminal surface is larger in case of large domes. The flow becomes stagnant at the apex of the dome and hence the low WSS developed at the top of the dome. Figure 8 also shows the increase in wall shear stress at a very small region at the distal side of the aneurysm neck where the flow impact is observed. The blood flow from the inlet impinges on the neck of the aneurysm which causes high-velocity gradient near the wall. This causes high WSS at the neck. Also, higher velocity gradients produced from secondary flow develops high WSS at the distal side of the neck. WSS less than 0.4 Pa covers large areas of the sac, clinical studies suggest that atherosclerosis changes are predominant in the aneurysm wall at low WSS regions. This may be related to the development of aneurysms.

Figure 9 shows the bar chart highlighting the maximum and minimum WSS (averaged about the wall of the artery). The maximum WSS occurs at the neck where the fluid impinges the wall and gets divided into the aneurysm and the downstream of the parent artery. Quantitatively the variation is not very significant between the models as observed in Figure 9(a). However, there is significant variation of minimum WSS between different models as shown in Figure 9(b) which can be attributed to low velocity and which may be related to rupture of the aneurysm. The degeneration of the aneurysm wall increases from neck to the dome and some pathological studies have shown that rupture commonly occurs at the top of the aneurysm dome where the WSS is the lowest [31]. Figure 10 shows the area-averaged WSS for different aneurysm models. It can be observed that the average WSS taken over the aneurysm dome area reduces with increase in dome size. The presence of minimum WSS inside the aneurysm tends to increase the degeneration of the aneurysm wall. 92.6% reduction in WSS is observed in the aneurysm model of D/N = 1.5 and the reduction is higher in case of larger dome sizes. There is a 96.3% reduction in WSS is observed in the model of D/N = 2.5.

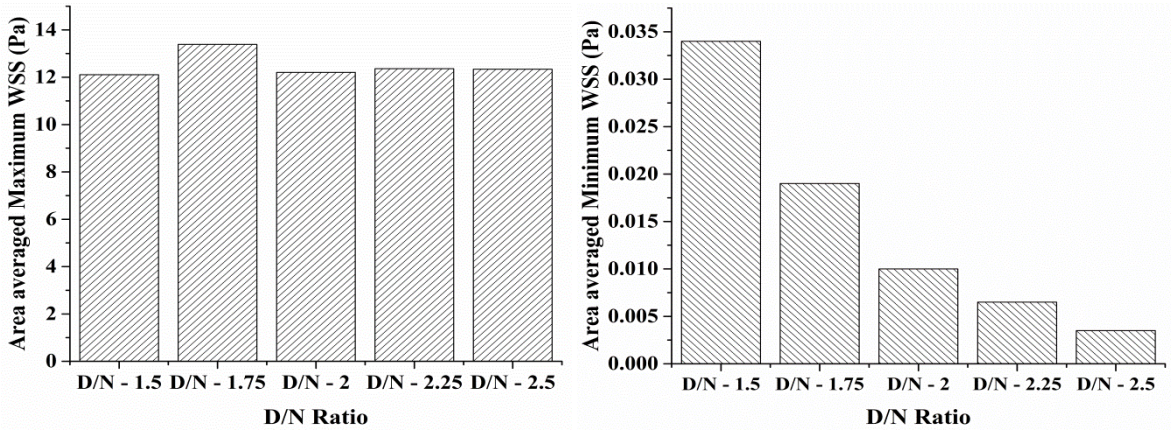

Figure 9. (a) Area averaged maximum WSS, (b) Area averaged minimum WSS

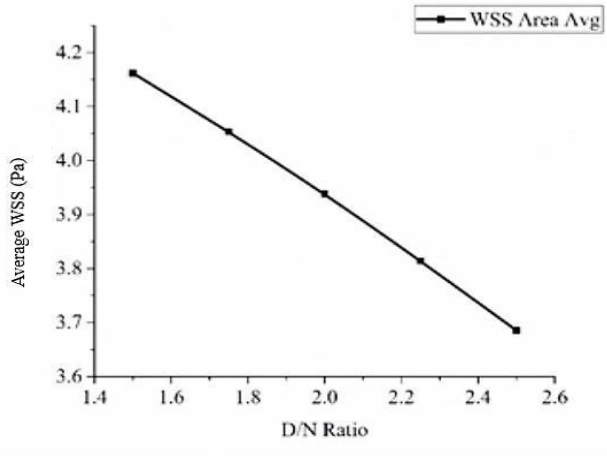

Figure 10. Average of WSS at the aneurysm area for different aneurysm modes

The velocity profiles at the neck of the aneurysm models are shown in Figure 11. It is interesting to observe that the velocity profiles are approximately the same for all the models. The results also show that the inflow in the aneurysm does not depend on the shape of the aneurysm.

Table 3 represents the percentage reduction of minimum velocity and minimum WSS near the wall-plane interface location. There is a significant reduction in minimum WSS at the top region of the aneurysm dome. The reduction of minimum velocity and WSS is higher for the models with higher D/N ratio. Similarly, the percentage reduction in average velocity and WSS calculated over the aneurysm area is shown in Table 3. There is a significant reduction in average velocity and WSS. These values are higher with the higher D/N ratio models.

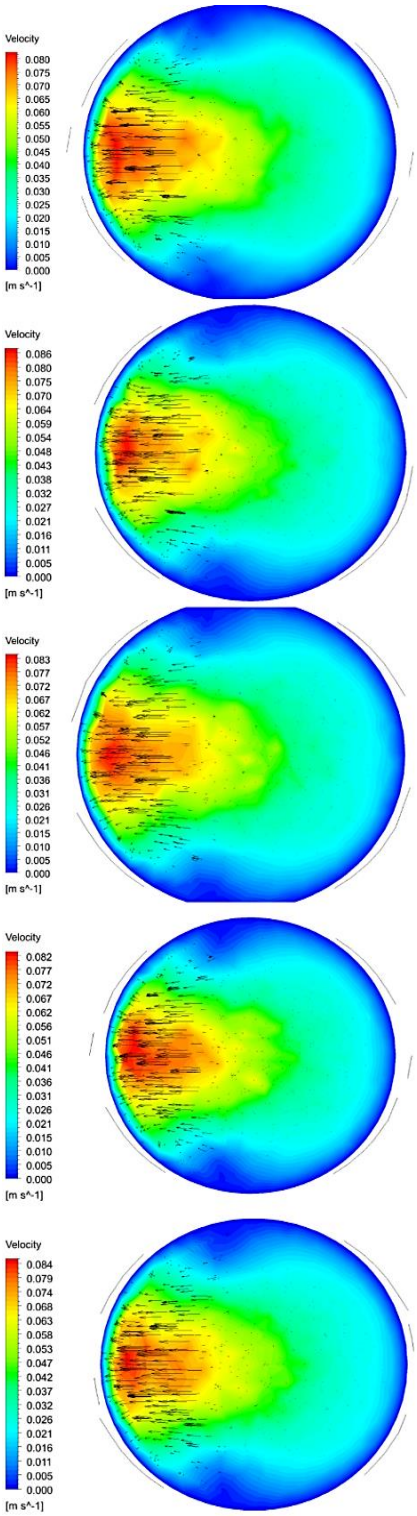

Figure 11. Velocity vector and velocity contours at the neck of the aneurysm

Table 3. Reduction in velocity and wall shear stress parameters inside the aneurysm

Model	Near the wall-plane interface		Over the aneurysm area	
	Reduction in maximum velocity (%)	Reduction in minimum wall shear stress (%)	Reduction in average velocity (%)	Reduction in average wall shear stress (%)
D/N - 1.5	94.5	95.6	94.6	92.6
D/N - 1.75	95.2	96.1	95.1	93.8
D/N – 2	95.8	96.8	95.9	94.7
D/N - 2.25	96.7	97.4	96.5	95.5
D/N - 2.5	97.3	97.9	97.0	96.3

CONCLUSIONS

Idealised aneurysm model of different dome sizes was used to study the flow dynamics. Variation of hemodynamic parameters such as velocity, wall shear stress and vortex structure is observed in the study. The results highlight the importance of the aneurysm size to determine the intra-aneurysmal hemodynamics. To determine indices for clinical diagnosis of aneurysms, the large number of results from parametric studies and clinical studies is necessary. Parametric studies can be readily performed using the present models.

The flow from the main artery enters into the aneurysm along the upstream side. For the model with lower D/N ratio, the flow is more hence creates a larger inflow contour. The flow gradually decreases for the models of higher D/N ratio. There is a significant reduction of 94% in minimum and average velocity is found inside the aneurysm. About 95% of reduction in minimum WSS and 93% of reduction in average wall shear stress is observed inside the aneurysm. This reduction of velocity and wall shear stress is increasing with the increase in dome size. Minimum WSS is an important factor in the growth and rupture of the aneurysm due to the development of atherosclerosis.

The flow impact is on the distal side of the neck and as a result of which there will be higher wall shear stress. 60% higher wall shear stress is observed at a small region on the distal side. High wall shear stress is considered to be a predominant factor in the initiation of the aneurysm. A part of the flow is directed towards the dome and lower wall tension and wall shear stress are present inside the dome. There are no significant differences observed on the inflow pattern of blood into the aneurysm. Hence inflow into the aneurysm does not depend on the shape of the aneurysm.

REFERENCES

[1] B. Weir, "Unruptured intracranial aneurysms: a review," *J. Neurosurg.*, vol. 96, no. 1, pp. 3–42, 2002.

[2] G. Mulder, A. C. B. Bogaerds, P. Rongen, and F. N. van de Vosse, "On automated analysis of flow patterns in cerebral aneurysms based on vortex identification," *J. Eng. Math.*, vol. 64, no. 4, p. 391, 2009.

[3] Y. Hoi *et al.*, "Effects of arterial geometry on aneurysm growth: three-dimensional computational fluid dynamics study," *J. Neurosurg.*, vol. 101, no. 4, pp. 676–681, 2004.

[4] K. Sato, Y. Imai, T. Ishikawa, N. Matsuki, and T. Yamaguchi, "The importance of parent artery geometry in intra-aneurysmal hemodynamics," *Med. Eng. Phys.*, vol. 30, no. 6, pp. 774–782, 2008.

[5] Y. Imai, K. Sato, T. Ishikawa, and T. Yamaguchi, "Inflow into saccular cerebral aneurysms at arterial bends," *Ann. Biomed. Eng.*, vol. 36, no. 9, p. 1489, 2008.

[6] J. L. Thenier-Villa *et al.*, "Hemodynamic changes in the treatment of multiple intracranial aneurysms: A computational fluid dynamics study," *World Neurosurg.*, vol. 118, pp. e631--e638, 2018.

[7] T. Sano, F. Ishida, M. Tsuji, K. Furukawa, S. Shimosaka, and H. Suzuki, "Hemodynamic differences between ruptured and unruptured cerebral aneurysms simultaneously existing in the same location: 2 case reports and proposal of a novel parameter oscillatory velocity index," *World Neurosurg.*, vol. 98, pp. 868--e5, 2017.

[8] M. Meuschke, S. Voß, B. Preim, and K. Lawonn, "Exploration of blood flow patterns in cerebral aneurysms during the cardiac cycle," *Comput. Graph.*, vol. 72, pp. 12–25, 2018.

[9] L. Xu, B. Zhao, X. Liu, and F. Liang, "Computational methods applied to analyze the hemodynamic effects of flow-diverter devices in the treatment of cerebral aneurysms: Current status and future directions," *Med. Nov. Technol. Devices*, vol. 3, p. 100018, 2019.

[10] G. Janiga, L. Daróczy, P. Berg, D. Thévenin, M. Skalej, and O. Beuing, "An automatic CFD-based flow diverter optimization principle for patient-specific intracranial aneurysms," *J. Biomech.*, vol. 48, no. 14, pp. 3846–3852, 2015.

[11] P. Goswami, D. K. Mandal, N. K. Manna, and S. Chakrabarti, "Numerical investigations of various aspects of plaque deposition through constricted artery," *J. Mech. Eng. Sci.*, vol. 13, no. 3, pp. 5306–5322, 2019.

[12] T. Hassan, Y. M. Ahmed, and A. A. Hassan, "The adverse effects of flow-diverter stent-like devices on the flow pattern of saccular intracranial aneurysm models: computational fluid dynamics study," *Acta Neurochir. (Wien).*, vol. 153, no. 8, pp. 1633–1640, 2011.

[13] Y. H. Kim, X. Xu, and J. S. Lee, "The effect of stent porosity and strut shape on saccular aneurysm and its numerical analysis with lattice Boltzmann method," *Ann. Biomed. Eng.*, vol. 38, no. 7, pp. 2274–2292, 2010.

[14] M. H. Babiker, L. F. Gonzalez, F. Albuquerque, D. Collins, A. Elvikis, and D. H. Frakes, "Quantitative effects of coil packing density on cerebral aneurysm fluid dynamics: an in vitro steady flow study," *Ann. Biomed. Eng.*, vol. 38, no. 7, pp. 2293–2301, 2010.

[15] C. F. Gonzalez, Y. I. Cho, H. V Ortega, and J. Moret, "Intracranial aneurysms: flow analysis of their origin and progression.," *Am. J. Neuroradiol.*, vol. 13, no. 1, pp. 181–188, 1992.

[16] N. F. Kassell and J. C. Torner, "Size of intracranial aneurysms," *Neurosurgery*, vol. 12, no. 3, pp. 291–297, 1983.

[17] L. Parlea, R. Fahrig, D. W. Holdsworth, and S. P. Lownie, "An analysis of the geometry of saccular intracranial aneurysms," *Am. J. Neuroradiol.*, vol. 20, no. 6, pp. 1079–1089, 1999.

[18] H. Ujiie, Y. Tamano, K. Sasaki, and T. Hori, "Is the aspect ratio a reliable index for predicting the rupture of a saccular aneurysm?," *Neurosurgery*, vol. 48, no. 3, pp. 495–503, 2001.

[19] Y. Hoi, S. H. Woodward, M. Kim, D. B. Taulbee, and H. Meng, "Validation of CFD simulations of cerebral aneurysms with implication of geometric variations," *J. Biomech. Eng.*, vol. 128, no. 6, pp. 844–851, 2006.

[20] K. Sudo, M. Sumida, and R. Yamane, "Secondary motion of fully developed oscillatory flow in a curved pipe," *J. Fluid Mech.*, vol. 237, pp. 189–208, 1992.

[21] A. J. Geers, I. Larrabide, H. G. Morales, and A. F. Frangi, "Approximating hemodynamics of cerebral aneurysms with steady flow simulations," *J. Biomech.*, vol. 47, no. 1, pp. 178–185, 2014.

[22] J. P. Ku, C. J. Elkins, and C. A. Taylor, "Comparison of CFD and MRI flow and velocities in an in vitro large artery bypass graft model," *Ann. Biomed. Eng.*, vol. 33, no. 3, pp. 257–269, 2005.

[23] A. Sherikar and P. J. Disimile, "RANS study of very high Reynolds-number plane turbulent Couette flow," *J. Mech. Eng. Sci.*, vol. 14, no. 2, pp. 6663–6678, 2020.

[24] N. Kumar, A. Khader, R. Pai, P. Kyriacou, S. Khan, and P. Koteshwara, "Computational fluid dynamic study on effect of Carreau-Yasuda and Newtonian blood viscosity models on hemodynamic parameters," *J. Comput. Methods Sci. Eng.*, vol. 19, no. 2, pp. 465–477, May 2019.

[25] V. Mendez, M. Di Giuseppe, and S. Pasta, "Comparison of hemodynamic and structural indices of ascending thoracic aortic aneurysm as predicted by 2-way FSI, CFD rigid wall simulation and patient-specific displacement-based FEA," *Comput. Biol. Med.*, vol. 100, pp. 221–229, 2018.

[26] E. A. Kosasih, R. F. Karim, J. Julian, and others, "Drag reduction by combination of flow control using inlet disturbance body and plasma actuator on cylinder model," *J. Mech. Eng. Sci.*, vol. 13, no. 1, pp. 4503–4511, 2019.

[27] N. Kumar, S. M. A. Khader, R. Pai, S. H. Khan, and P. A. Kyriacou, "Fluid structure interaction study of stenosed carotid artery considering the effects of blood pressure," *Int. J. Eng. Sci.*, vol. 154, p. 103341, 2020.

[28] Y. Zhang *et al.*, "Hemodynamic effects of stenting on wide-necked intracranial aneurysms," *Chin. Med. J. (Engl).*, vol. 123, no. 15, pp. 1999–2003, 2010.

[29] H. Ujiie *et al.*, "Effects of size and shape (aspect ratio) on the hemodynamics of saccular aneurysms: a possible index for surgical treatment of intracranial aneurysms," *Neurosurgery*, vol. 45, no. 1, pp. 119–130, 1999.

[30] A. M. Malek, S. L. Alper, and S. Izumo, "Hemodynamic shear stress and its role in atherosclerosis," *Jama*, vol. 282, no. 21, pp. 2035–2042, 1999.

[31] J. R. Cebral, M. Sheridan, and C. M. Putman, "Hemodynamics and bleb formation in intracranial aneurysms," *Am. J. Neuroradiol.*, vol. 31, no. 2, pp. 304–310, 2010.